Computer Simulation: Biomolecules on Surfaces

Filipe Camargo Dalmatti Alves Lima, Luana Sucupira Pedroza, Rodrigo Garcia Amorim, and Wanderlã Luis Scopel

1 Introduction

Most chemical and physical properties of atomic systems are related to electronic properties. Those properties are still one of the most studied topics since they can behave differently among molecules, solids, interfaces, and their interactions. In the last decades, experimental techniques became more sophisticated, being able to reach the electronic structure and to provide unique fingerprints. One of the hot topics studied is surface science, due to its large area leading to a potential for applications, such as biomolecule identification. Due to the experimental challenges, one way to have better comprehension of quantum effects at surfaces is using theoretical modeling. In particular, Density Functional Theory (DFT) is a powerful tool to study the electronic structure, electron transfer, binding energies, electron transport, and currents, being able to provide further insights about these systems.

Surface modeling is a many-body problem that involves several atoms and electrons. In quantum mechanics, this type of problem does not have an analytical solution. Just a few simple problems have an analytic solution: a free particle in a box, quantum oscillator, and hydrogen atom. The first approximation that can be done to

F. C. D. A. Lima (✉)
Federal Institute of Education, Science, and Technology of São Paulo (IFSP), Matão, SP 15991-502, Brazil
e-mail: fdlima@ifsp.edu.br

L. S. Pedroza
CCNH - Center for Natural Sciences and Humanities, Federal University of ABC (UFABC), Santo André, SP 09210-580, Brazil

R. G. Amorim
Physics Department, ICEx, Fluminense Federal University (UFF), Volta Redonda, RJ 27213-145, Brazil

W. L. Scopel
Physics Department, Federal University of Espírito Santo, Vitória, ES 29075-910, Brazil

F. N. Crespilho (ed.), *Advances in Bioelectrochemistry Volume 1*,
https://doi.org/10.1007/978-3-030-94988-4_1

simplify the problem is using the Born-Oppenheimer approximation: the electrons have different time scale compared with the nuclei, due to their mass difference ($m_N \gg m_e$). Thus, it is possible to consider the nuclei fixed to solve just the electronic hamiltonian. Although this problem becomes simpler to deal with, it is still unsolvable. There are different methods to treat this problem based on wavefunction, that depends on 3N variables without considering the spin. An example of a wavefunction method is Hartree-Fock [60]. For large systems, this method is extremely costly. One way to overcome this very hard problem is using the charge density instead, which is more efficient to treat compared to wavefunction's method. DFT was proposed by Hohenberg and Kohn in 1964 [26], which drastically changes how the results from the quantum mechanics theory are obtained. In 1965, Kohn and Sham [28] proposed mapping of N-body problem in N problems of one body. For that, they proposed the self-consistent equations and defined the KS potential that has the external potential, Hartree, and the exchange-correlation potential, which are known as Kohn-Sham Scheme (KS) for the DFT (KS-DFT).

The KS wavefunctions can be described using different mathematical approaches. There are many computational codes available that have a particular description, having some characteristics with advantages and disadvantages. Computational codes such as Gaussian [17] or ORCA [43] employ wavefunctions based on Pople's Gaussian orbitals in real space, being very effective to describe molecular structures, however struggles to study bulk materials or molecule/material interfaces. Quantum ESPRESSO [14, 20] and VASP [29] on the other hand, describe the wavefunctions as planewave basis sets in reciprocal space, using pseudopotentials [62] or projector augmented wave (PAW) [6] approximations to describe the core region of the atoms. While reciprocal space methods are well suited for bulk materials and interfaces, their computational cost is hugely increased in comparison to real space methods. There are also computational codes such as SIESTA [18] that employs numerical localized basis sets, pseudopotentials and linear-scaling algorithms in real space, allowing investigations of molecules, bulk material and interfaces. In the end, the computational packages choice is based on which property of interest, or the type of material, is investigated. There are state-of-art theories and computer implementations that are exclusive to it package.

Another critical point to establish the DFT accuracy, precision and reliability is the exchange correlation functional (E_{xc}) employed for the system. The most common used in the electronic structure calculations are the Local Density Approximation (LDA) [48], generalized gradient approximations (GGA) such as PBE [49] or PBEsol [50], and hybrid functionals such as B3LYP [5] or HSE [25]. If a system has non-bonded interactions, van der Waals corrections should be included [21]. As discussed before, there is not an unique choice since it depends on the system model, the analysis, the computational code, convergence tests and the computational resources available. There are many studies that provide E_{xc} benchmarks, for example Su et al. [59].

The analysis of the electronic structure calculations allows to understand the stability, bonding, potential energy surface, density of states (DOS), band structure, electronic transport and others properties for different systems. The highlight proper-

ties could guide and/or support the experimental results, leading to the understanding of fundamental atomic aspects.

The KS wavefunctions are the eigenvectors obtained from the KS equation, associated with the energy levels/bands, that express the probability to find an electron in a given region of the space. They can be used to understand where the electrons are localized in the molecule/solid and how they can behave. In bioelectrochemistry, this analysis can help to understand which atoms can possibly participate on the electron transfer process between the surface and molecule.

The DOS accounts the electronic states that are found in a particular energy, or in an energy window. It can be related to physical or chemical effects, such as surface interactions, reaction centers, defects, electron entrapment and others. Also, it can be used to reproduce experimental techniques such as scanning tunneling microscopy (STM). The total DOS for a given system is difficult to interpret since there are many states involved. In this scenario, projected DOS for a given atom and/or orbitals, or atomic groups are employed instead. This helps to understand the specific role for the components of the system.

The electronic transport is a powerful model to understand microscopically what is happening in a electrochemistry process and nanodevices such as biosensors, etc. The concept of the electronic transport is different of canonical electronic calculation in equilibrium. In this case, two electron reservoir or electrodes are considered, and the central region is called the scattering region. There is one electrode in the left side and other in the right of the scattering region. The system is considered semi-infinity in both directions [7, 54]. The basic quantity calculated is the transmission function, that represents the probability of one electron, from the left side, to reach the right electrode passing through the scattering region. The transmission relevance is due to the possibility to obtain the electronic conductance and current. In the case of biosensors, one can calculate the transmission for the bare system and to obtain the zero bias conductance/resistance. For the molecule chemio/phisiosorbed in the device, it is possible to calculate the new transmission, where the charge transfer between the molecule and device will play the main role. Changes in the conductivity/resistance (sensitivity) can be a powerful tool to identify electrical signature of biomolecules in such systems.

The molecule adsorption can be understood by the total charge density that is given by the square of KS wavefunctions. The charge density gives the electron probability and possibly quantifies the referred property. For example, in a pristine material, the charge density can characterize the bond nature. If the system is composed by a surface and a molecule, it is possible to evaluate the electronic charge reorganization through the charge density difference. In this case, we consider the difference between the whole system (surface + molecule) and isolated counterparts. From the mathematical point of view, it is possible to write:

$$\Delta\rho(\vec{r}) = \rho_{surface+molecule}(\vec{r}) - (\rho_{surface}(\vec{r}) + \rho_{molecule}(\vec{r})), \tag{1}$$

where the regions can be locally analyzed: in the case of $\Delta\rho(\vec{r}) > 0$, that region decreases the charge, and for $\Delta\rho(\vec{r}) < 0$, the charge increases when compared to

the isolated parts. This quantity gives how the charge is redistributed in the entire system compared with the isolated ones. The charge redistribution is an important way to quantify the charge transfer between molecule and surface.

Richard Bader [4] has proposed an intuitive scheme for visualization of atoms in molecules focusing on the charge density. Bader has used zero flux surfaces to separate the atomic charge, where the electronic charge density has a minimum value perpendicularly to the surface. Typically in molecular systems, the charge density reaches a minimum between neighbour atoms, which is a natural place to separate them from each other. Therefore, Bader considered the electronic charge density enclosed within this volume as a good approximation for the total electronic atom charge. Thus, obtaining the partial atomic charges. This quantity is interesting to investigate local reorganization, reduction and oxidation states in the bioelectrochemistry context. For computational Bader charge analysis, there is a open source code developed by Henkelman Group [24, 66].

In the following sections, we illustrate the state of the art of theoretical models of biomolecules interface with surface or nanodevices. These systems were treated within quantum mechanics calculations, using the analysis tools summarized here.

2 Electron Transfer of Peptide SAMs Modified with Ferrocene

The heterogeneous electron transfer (ET) involves a molecule/electrode interface that is composed by a donor-acceptor system: the electroactive group is connected to the electrode through a spacer molecule, which can be a polypeptide, alkanethiol, lipid, sugar, and others. In particular, ferrocene (Fc) modified self-assembled monolayers (Fc-SAMs) have been considered as excellent models for the study of ET [13, 40, 55]. One interesting study has observed higher ET rate in peptides compared to thiol ligand, both functionalized with Fc [45]. Despite the progress in the area, there is a dichotomy regarding the ET mechanism [38]: from one side they believe that the electron hopping through amide groups whereas the electron moves within sites from the donor to the acceptor; on other hand, electron tunneling where the electron moves from the donor to acceptor without any intermediate state.

Based on this paradigm, the community carried out new experiments [13, 27, 37, 39, 42, 47, 51, 55, 61, 65], emerging three possible types of ET mechanisms: molecular mobility, electron tunneling, and hopping, as well as combinations of those [8, 39, 61].

From the theoretical perspective, Lima et al. [33] carried on DFT calculations of several models to investigate each component in the system. For calculations, the authors used DFT and GGA exchange-correlation functional, other computational details can be found elsewhere [33]. These tests investigated the role of the space molecule glycylcistamine (Gly-CSA), the electroactive center Fc and the electrode modeled by the Au(111) surface. It is worth to observe that the electronic states that

belongs to the Gly-CSA are always below the Fermi energy, even during simulation considering Gly-CSA@Au(111). On the other hand, the Fc electronic states are always located close to the Fermi energy, regardless the configuration it was investigated. In summary, Fig. 1 shows a gold slab with the Fc-SAMs with the organic solvent environment. The DOS analysis in this case indicates the electronics states closer to the Fermi Energy (E_F) are the thiol bond (S-Au), then the Fc group (H_M) without any intermediate state from the spacer (H_m) or the solvent. In terms of the energetics, while the Fc peak is placed at -0.3 eV, the electronic contributions for the molecular spacer are located about -1.5 eV below the E_F. Although DFT simulations presented do not show the dynamics of ET, the results demonstrate the electronic pathways. In this case, it is possible to describe the ET involving the Fc group and the gold electrode, favoring the electron tunneling mechanism. The DOS analysis combined with different building models contributed to elucidate the charge mechanism discussion in Fc-SAMs.

3 Two-Dimensional (2D) Systems

In 2004, graphene mechanical exfoliation was assembled by Geim and Novoselov [44], opening new perspectives in 2D materials and its applications. Graphene is a lightweight, atom-thick, zero-gap semiconductor, it has a large Young's Modulus (about 1 TPa) that is flexible perpendicularly to its basal plane. These unique properties in a single material make it special among others. One of the promising applications of graphene is using as a fast biomolecule sensor, i.e. utilize it as a solid-state nanodevice for electric identification. Graphene paves the way for 2D materials [16], and nowadays more than 700 different structures are known. It is possible to highlight some of 2D materials such as: h-BN [3], silicene [2], germanene [34], borophene [64], phosphorene [10], transition metal chalcogenides (TMDs) [12], Janus [67], also combinations of them (hybrid materials) [22, 56, 58]. Considering the electrical properties, the 2D materials can be metallic, semi-metallic, semiconductor and insulator. The material properties control allows different technological applications e.g.: biosensors, next generation batteries and nanodevices.

For biomolecule electric sensing, there are three possible mechanisms discussed by Heerema [23] and Diventra [11], where the schematics are depicted in Fig. 2: (a) on top, (b) on edge or nanogap and (c) nanopore device, respectively.

On top mechanism uses a large 2D surface area for device biomolecule identification. In this mechanism, the molecule is lying on the surface as could bind strongly (chemisorbed) or weakly (physisorbed), depending on the molecule nature. In general, the device has a bare resistance, and each molecule has different electron transfer. This charge transfer and perturbation leads to changes in the device resistances, thus the sensitivities can be characterized. A typical biomolecular signature is the Fano resonances [41], and the challenge is to distinguish a molecule among others based on their signal. Another important aspect to be considered for the nanodevices consists to detect the biomolecules with binding energies smaller than 1.0 eV. The

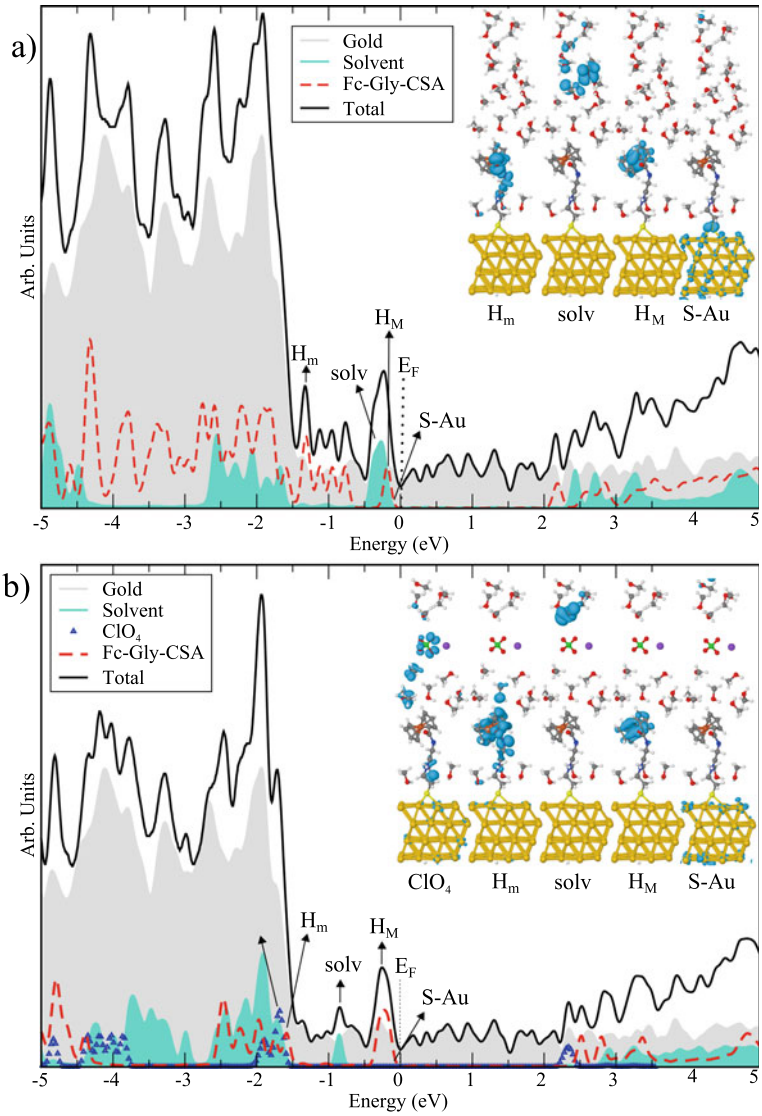

Fig. 1 Total DOS (black line) and projected contributions on the Au substrate (shaded area) and Fc-Gly-CSA molecule (red line) for the molecule/surface interface: **a** including methanol solvent (cyan area); **b** including sodium perchlorate (blue line) and methanol solvent. Zero energy reference is set to the Fermi energy (E_F) of the system. Insets display representative single particle orbitals of the interface. Reprinted (adapted) with permission from Ref. [33]. Copyright 2014, American Chemical Society

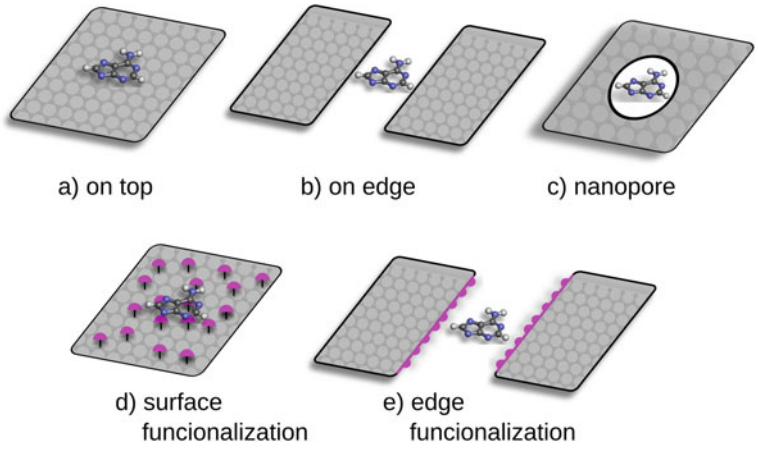

Fig. 2 Systems based with graphene, with possible site interactions: **a** on top; **b** on edge or nanogap; **c** nanopore; **d** surface functionalization; **e** edge functionalization

translocation time is given by $\tau \sim \exp(\frac{-E_b}{K_B T})$, where E_b is the binding energy, K_B is the Boltzmann constant and T is temperature, that characterize the molecule resident time in the device. Large binding energies could lead to disposable nanodevice, once the translocation time could be very large. For the case of very small molecule binding, it is possible to consider the surface functionalization as it is shown in Fig. 2d. The functionalization should be an atom or a molecule that acts an anchor to interact with the biomolecule.

Figure 2b is shown on edge or nanogap device based on tunneling mechanism. For a bare system, the transmission is zero per construction due to the large distance between the sides. When the molecule is placed on the nanogap, it can work as a bridge between the two sides (electrodes) and the electron could tunnel from the left to the right side. The conductance typical signal is about 10^{-10} G_0 and this fact could be a experimental challenge due to the signal-to-noise ratio. A possible way to minimize this problem is the edge functionalization with different atoms as it is shown in Fig. 2e. The functionalization can increase the conductance signal and signal-to-noise ratio. This fact could improve the tunneling transmittance signal for different biomolecule, that also depends on the coupling.

The nanopore is the third and more promising biomolecule nanodevice as it is shown in Fig. 2c. In this case, there are a nanodevice with 10–20 Å pore diameter. This pore size allows the biomolecule passing through it, changing the electronic characteristics of system. In this mechanism the bare device has a resistance, when the molecule is inside the pore it changes, which is similar to the on top. In fact, the molecule can modulate the electronic current leading to its identification. Nowadays, there are technics to control the nanopore size, shape and its functionalization, fundamental for this type of applications.

In the next sections, the three mechanism will be exemplified in the detection of nucleobases, also discussing the aspects regarding the change transfer, that is a possibility to identify each one.

3.1 On Top Application Using Silicene

Silicene is a silicon 2D material, similar to graphene, with honeycomb lattice that was proposed theoretically by Ciraci et al. [9]. The electronic structure is a semimetal system with a Dirac cone in K-K'-symmetry point, similar to graphene. However, silicene is buckled and more stable than planar structure by 0.05 eV [2]. This fact is due to $sp^2 - sp^3$ bonds, that leads to the referred roughness. The lattice parameter for buckled (planar) is about 4.002 (3.995) Å with 0.55 Å of height, using DFT and GGA + van der Waals correction for exchange correlation functional as implemented in SIESTA code. Further details can be find elsewhere [2]. Considering the transport point of view, it was build a supercell that are coupling two electrodes in left/right sides. The transmission gives a V-shape curve, in good agreement to Dirac materials. Biomolecules such as: adenine (A), cytosine (C), guanine (G) and thymine (T), were adsorbed on the silicene surface and distinct orientations were fully relaxed. With the most stable geometries of each nucleobase were calculated the binding energy and the distance between the molecule and device. For A and T, the distance was about 3.0 Å and the binding energy close to -0.6 eV. However, for C (G) the distances were about 2.0 Å and the binding energy were -0.88 (-0.77 eV), respectively. The strong binding for C and G is related to single oxygen atom presented in each nucleobase. This fact makes the molecule tilt, where the Si-O atoms are minimal distance between the surface and biomolecule. For A and T the molecules are planar, where the A does not have oxygen atoms, and T has two (one in each molecule side). For the T molecule, there are oxygens competition and the molecule stays quasi planar. Based on these results, it is possible to classify the nucleobase in two groups: (I) weak binding (A and T) molecules and (II) strong binding (C and G).

Figure 3 shows the difference of charge density calculated using Eq. 1. For the group I, it is noted a charge repulsion between the biomolecule and the silicene device. For A and T (Fig. 3a, d), the negative difference (blue color) is between the bottom of the molecule and the surface. In another hand, Fig. 3b, c represent the group II, where the molecules (C and G) are stronger in terms of binding energy, leading to an attractive charge redistribution. In the inset, can be noted a negative charge concentration between Si-O and a positive charge on Si atoms, confirming this assumption. These results confirm the binding energy previously discussed.

Next, we analyse the electronic transport by the transmission function. For C and G molecule, it was noted a decreasing in the transmission at $+1.0$ eV, compared with pristine device and also A and T. A similar result is also noted from -1.0 eV to E_F, where the group II decreases the transmission compared to the pristine one. Fano resonances were observed for energies smaller than -1.0 eV, typical from molecular signatures. For the inset upper (lower), two energies were chosen for the

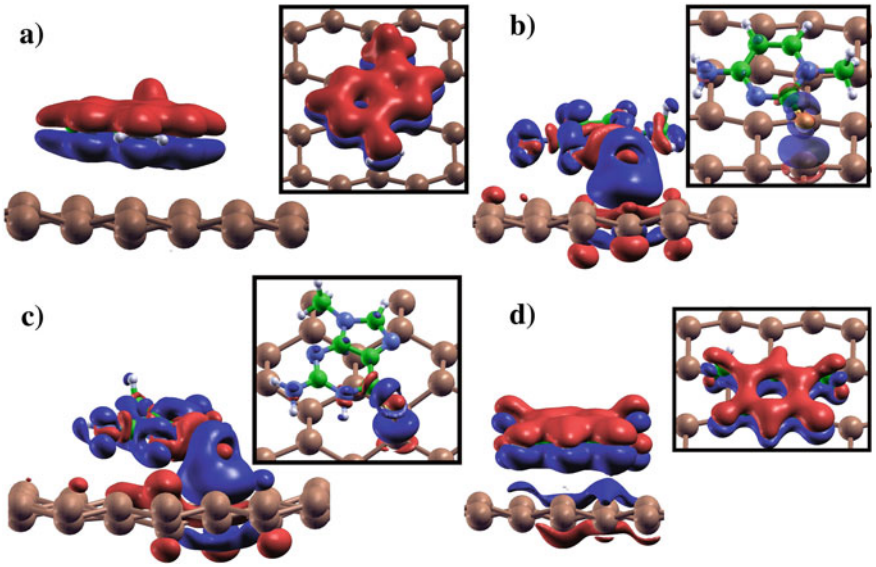

Fig. 3 The change in electronic charge density is plotted, calculated as the difference between the charge density of the total system (silicene + nucleobase) and that of each constituent part (silicene, nucleobase) separately. Blue color indicates a negative difference in the charge density; red color indicates a positive difference in the charge density. The main panels show isosurfaces for a value of 0.001 electron $\times$ bohr^{-3} while the insets show the same charge density difference data plotted for a larger isosurface value of 0.03 electron $\times$ bohr^{-3} and viewed from a different perspective. **a** Adenine; **b** cytosine; **c** guanine; **d** thymine. Reprinted (adapted) with permission from Ref. [2]. Copyright 2015, IOP Publishing, Ltd.

analysis of the changes in the transmission. In both cases, the molecules transmission are different than the pristine one. The transmission changes observed leading to the modification in the resistance/conductance, important aspect to molecule identification.

For electrical nucleobase identification were chosen two energies values $+1.0$ eV and -1.26 eV (upper and lower right side panel on Fig. 4), at the Fano resonances. One way to identify changes in the conductance/resistence is through the sensitivity, that is given by:

$$S[\%] = \left(\frac{g_0 - g_i}{g_0}\right) \times 100, \tag{2}$$

where g_0 is the pristine conductance and g_i is the nucleobase conductance (for i = A, C, G and T). Figure 5 shows the sensitivity, where for a gate voltage of -1.26 eV is noted a sensitivity up to 20% to A and about 3% for T. The nucleobase C and G has similar sensitivities (around 10%). However, considering the gate voltage of $+1.0$ eV it is possible to identify C and G with a good resolution and A and T are indistinguishable. This device can identify each nucleobase using two gate voltages through sensitivities, as well as with translocation time with a good resolution.

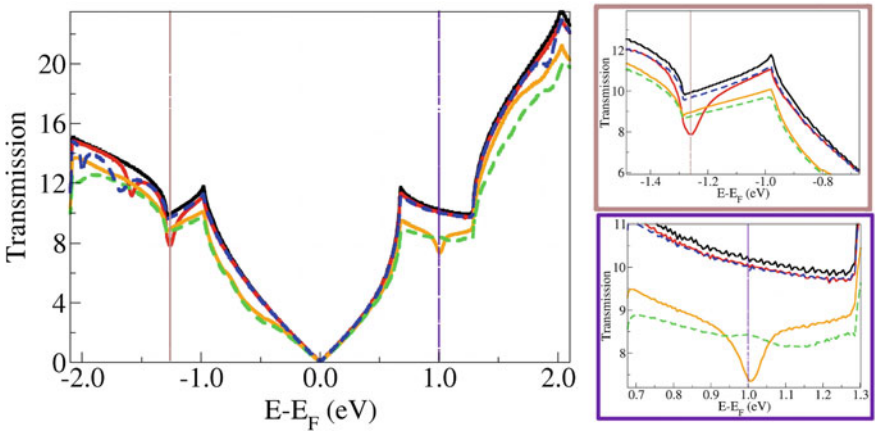

Fig. 4 The plot shows the zero-bias transmission of silicene with and without nucleobases on top as a function of the electron energy, with the Fermi level for the whole system aligned to 0 on the horizontal axis. The curve in black color represents the transmittance for pristine silicene without any nucleobases present while the other colors (red, orange, green, and blue) refer respectively to the transmission for each nucleobase (A, C, G, and T, in that precise order) physisorbed or chemisorbed on top of silicene. Reprinted (adapted) with permission from Ref. [2]. Copyright 2015, IOP Publishing, Ltd.

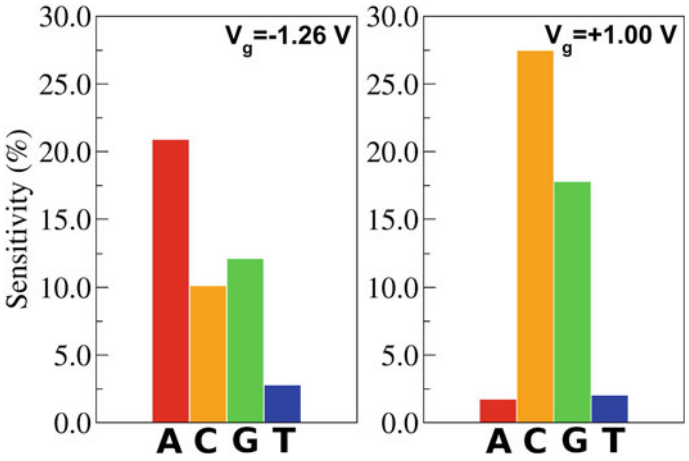

Fig. 5 For two different gate voltages (left panel: −1.26 V; right panel: +1.00 V) we plot the calculated sensitivity of the hypothetical silicene sequencing device with respect to the four different nucleobases A, C, G, and T). Reprinted (adapted) with permission from Ref. [2]. Copyright 2015, IOP Publishing, Ltd.

3.2 Nanogap Application with Graphene

Nanogap or edge device consists of surface material with a empty space between two regions. From the experimental point of view, Postma [52] proposed a graphene-based device for reading the transverse conductance of biomolecules, in particular nucleobases. In the proposed setup, it was considered the electrodes as the same material, demonstrating the nucleobase electrical detection with single-base resolution. Theoretically, a graphene nanogap device was investigated by Jariyanee Prasongkit et al. [53], where the tunneling transmission were studied, and the authors showed very small electrical conductance (in the order of $10^{-10}\ G_0$). The main question to be addressed consists on how can we modify the nanogap device to improve the transport properties. To answer this issue, the nanogap functionalization will be addressed to electrically detect biomolecules with better conductance signal.

The results shown here were obtained using DFT calculations with GGA exchange-correlation functional, further details can be found elsewhere [1]. Graphene nanogap with H- or N-edge functionalization were considered. The devices were built and full ionic relaxation were performed. Thus, the shortest distances between the two sides are about 13.85 Å. The A, C, G, and T nucleobases were placed as a linker between the two sites. There are two molecules that have two rings, namely group I (A and G), and two with one (C and T) as group II. For group II, it was expected that the small size, in comparison with group I, can lead to a weaker coupling. The nucleobases were relaxed inside the nanogap and for the group I were found distances smaller than group II for both devices.

Figure 6 shows the total density of charge for H- (left side), N-functionalized device (right side), and each row represents one nucleobase. The nitrogen is characterized by a high electron concentration (blue color) in comparison to the hydrogen one. Firstly, were observed a weaker coupling for the biomolecules of group II in contrast with the group I, as expected. In another hand, analyzing A as an example and comparing to a different device, were noted a strong interaction in a N-functionalized one. Figure 6 shows an inset in red for weak coupling (H-functionalized device) and N-functionalized the green/yellow. For A and C in H-functionalized devices, it is noted the smaller nucleobase presented a weaker interaction. This fact is also true for N-functionalized devices. However, for C in N-functionalized devices were observed a better electronic coupling in comparison with H-functionalized devices. These results show that group I has stronger coupling and the N-functionalized device is better for biomolecule detection in comparison to H one.

Figure 7a–b show the zero bias transmission for H-passivation (left panel) and N-passivation (right panel), respectively. Firstly, it was investigated the four nucleobases at each nanogap device. At Fermi energy, the transmission hierarchy was $G > A > C > T$ for both devices (-H and -N) and the main difference is the transmission order of magnitude. For N-functionalization it was noted a conductance improvement about $10^4 - 10^5\ G_0$. For all cases, there are resonances for a certain energy value due to the nucleobases. For nucleobase A, there is a peak at -1.0 eV for H-functionalized nanogap. Secondly, for N-functionalized devices, the previous peak moves towards

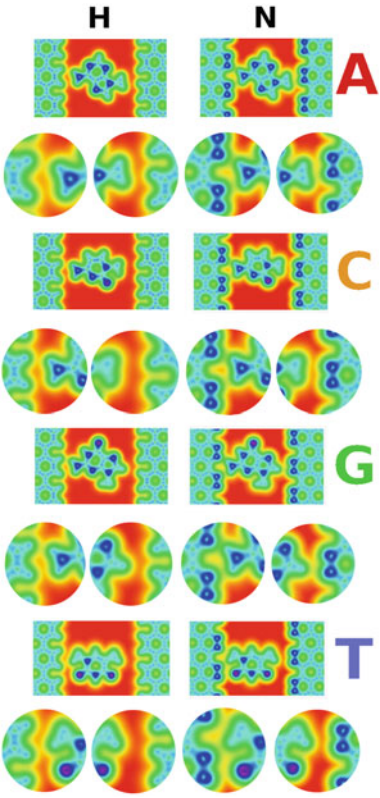

Fig. 6 Charge density for a graphene nanogap with nucleobase in between where left handside panel is for hydrogen, and right is for nitrogen functionalization. The circular insets show zoomed in regions at the frontier between molecule and edge. The colors represent the charge density is given in linear scale going from 0.0 (red) to 1.1 (violet) and $e/Bohr^3$. Reprinted (adapted) with permission from Ref. [1]. Copyright 2016 American Chemical Society

Fermi energy. This fact indicates that further device has a better coupling, as it was previously demonstrated in the total charge density analysis. When the molecules are placed in the N-functionalized material, there was noted a peak shift toward the Fermi energy.

For the nanogap case, the sensitivity characterization is difficult to evaluate due to zero transmission for the bare system (without the molecule). For the analysis of the changes in the conductance without device reference, it was considered a target molecule. In this case, it was chosen a molecule with the smaller conductance signal, which was the nucleobase T at the H-functionalized device. In this way, all nucleobase conductance were normalized by T, and the sensitivity definition is given by the following:

$$S[\%] = \left(\frac{g_i}{g_{ref}}\right) \times 100, \tag{3}$$

where g_i represents the nucleobase conductance, and g_{ref} the smaller conductance case (T in H-functionalized device). Figure 8 hashed histogram shows the H-functionalized, where the biggest sensitivity is given by G, followed by

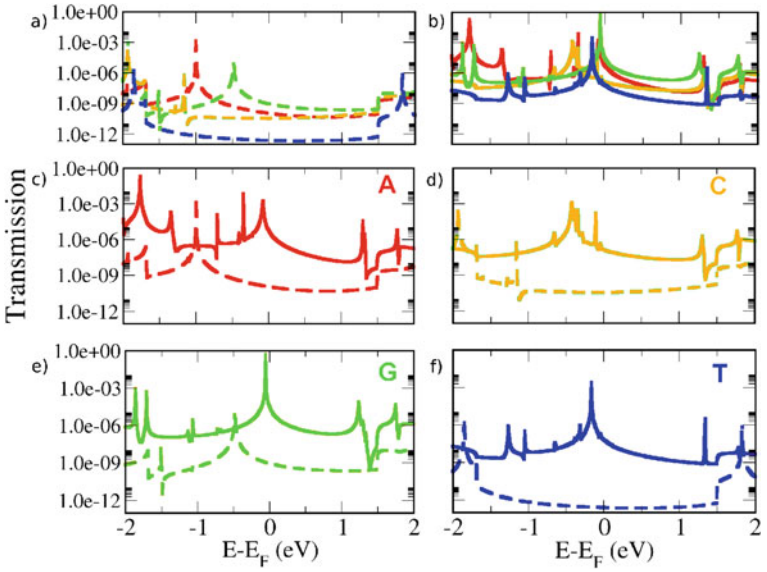

Fig. 7 Zero-bias transmission as a function of energy: graphene nanogap functionalized with **a** Hydrogen (dashed), and **b** Nitrogen atoms (solid) for all nucleobases; **c–f** transmittance comparison between H- and N-terminated edges of graphene nanogap with different nucleobases in between—A, C, G and T. Reprinted (adapted) with permission from Ref. [1]. Copyright 2016 American Chemical Society

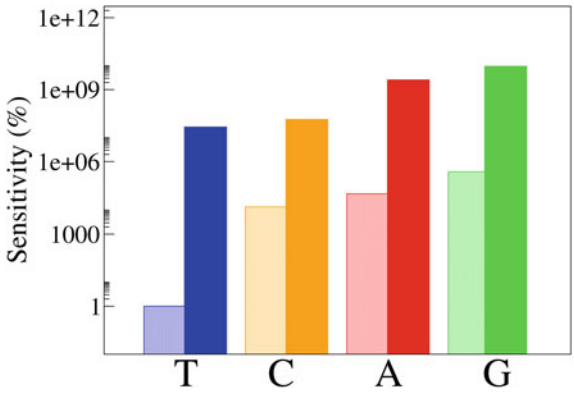

Fig. 8 Sensitivity at Fermi level of four nucleobases for H- (hashed) and N-functionalized (solid) nanogaps. Thymine in the H-terminated nanogap has the smallest conductance and was taken as a reference. Reprinted (adapted) with permission from Ref. [1]. Copyright 2016 American Chemical Society

A—nucleobases of group I, and C has a good resolution in comparison with T. Here, were demonstrated despite the small-signal the four nucleobases are distinguishable in H-functionalized device. Comparing the reference with an N-functionalized device, were noted an improvement in the sensitivity by more than five orders of magnitude, as well as the sensitivity follow the magnitude of the H-functionalized device ($G > A > C$).

3.3 Nanopore Application with Hybrid Graphene-BN Device

Nanopore inside of 2D materials has emerged as a great potential to be used as DNA sequencing due to its individual-base resolution. The applicability of solid-state nanopores for the detection and analysis of biomolecules is dependent on achieving accurate control of size and shape. In this context, recent advances in size and shape control have been achieved, using controlled dielectric breakdown [30] and electrochemical reaction (ECR) [15]. Encouraged by the experimental synthesis successfully of nanopores embedded in the 2D materials [15], Souza et al. [56], have been proposed a novel device based on lateral heterostructure graphene-BN.

For modeling the proposed systems herein, it was performed DFT calculation with GGA exchange-correlation functional, more details can be found somewhere [56]. The investigated setup has two electrodes (left and right) and a scattering region with a nanopore. The graphene stripe has a width of 16.92 Å embedded in the h-BN and the pore diameter is 12.5Å (see Fig. 9e). One important aspect of the device is the presence of two carbon nanowires (above and below the pore). Focusing on the electronic transport, Fig. 9a shows the transmission spectra for the bare device, where one should verify two broad peaks around the Fermi level in the energy range (± 0.25 eV)) and a well-defined peak at 0.9 eV. The transmission is actually not symmetric around the Fermi level. Figure 9b shows the vertical dashed lines (± 0.18 eV), where one can clearly note an asymmetric $T(E)$, as a result of the two distinct interfaces C1-B (C2-N), which present, electron acceptor (electron donor) character, respectively. In Fig. 9c the central peak (orange color) represents the total density of states (DOS) with the majority contribution ascribed to central carbon atoms (blue color, C). However, the left (right) shoulders are associated with the hybridized states from the interface atoms C1-B (C2-N), as highlighted in Fig. 9d. In order to get some insights about the $T(E)$ around the Fermi level, it was analyzed the local current in the scattering region at ± 0.18 eV. For the negative energy value (Fig. 9e), the local current is located in the lower carbon wire, while for the positive one (Fig. 6f) it is in the upper, as expected from the projected density of states (PDOS) (see Fig. 9c–d). The results reveal for the proposed device an important functionality, once it is possible to choose the electrons pathway switching the applied gate voltage.

The nucleobases were placed inside the nanopore and performed full relaxations. With the most stable configurations (Fig. 10a–d), the interaction strength between nanodevice and molecule were examined through the binding energy. Figure 10e shows binding energy for the four nucleotides such as: deoxyadenosine monophos-

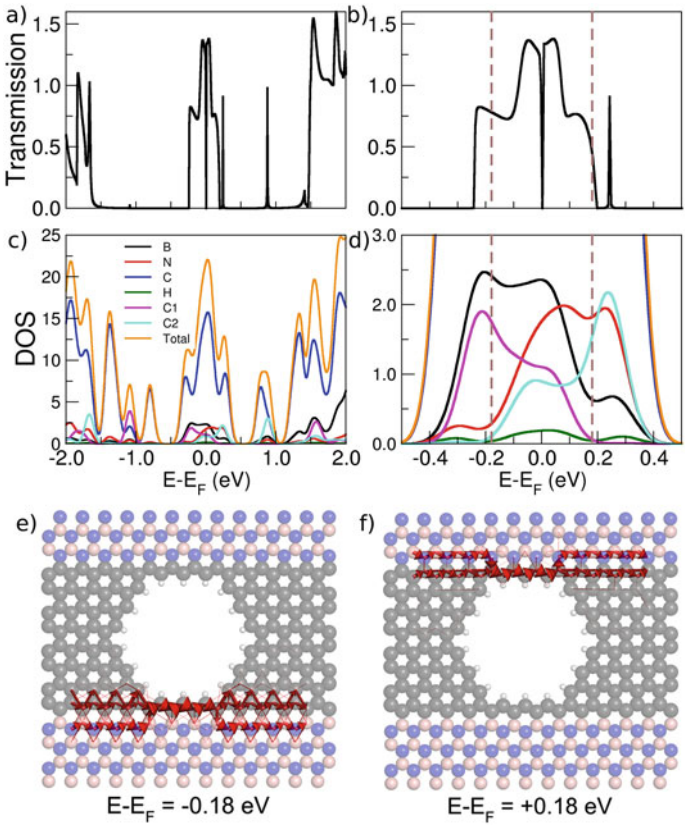

Fig. 9 **a** Zero-bias transmission spectra as a function of energy for the device without any molecule present in the pore; **b** zoom-in around Fermi level; **c** the projected density of states (PDOS) as a function of energy; **d** zoom-in of the PDOS around Fermi level; the local current density **e** for -0.18 eV and **f** for $+0.18$ eV. Reproduced from Ref. [56] with permission from the Royal Society of Chemistry

phate (dAMP), deoxyguanosine monophosphate (dGMP), deoxycytidine monophosphate (dCMP) and deoxythymidine (dTMP). In particular, the dCMP is 0.65 eV and dAMP is 0.13 eV, which is higher than corresponding binding energies on graphene and MoS_2 surfaces [31, 32]. Then, based on the binding energy values, one can infer that dCMP will have the biggest resident time while dAMP will have the smallest one. These results suggest that the device might also allow to identify individually different target molecules due to their specific residence times into the nanopore.

Figure 10f shows the transmission spectrum of the bare device (black dashed line) and device with four nucleotides. These results reveal that one can distinguish the nucleotides based on their transmission signature around the Fermi level. In general, one can observe that $T(E)$ decreases for all nucleotides relative to the bare nanopore system. However, for one case (i.e., dGMP), there is an electron channel opening for

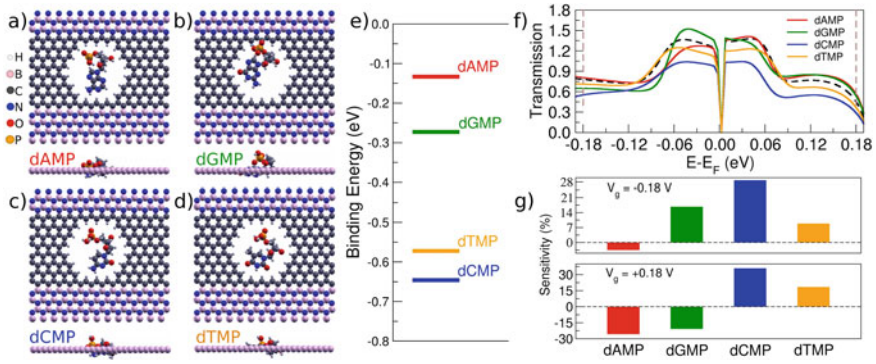

Fig. 10 Fully relaxed structures for each nucleotide **a** dAMP, **b** dGMP, **c** dCMP, and **d** dTMP inside the pore; **e** binding energies; **f** zero-bias transmission spectra in the vicinity of the Fermi level for the empty pore (black dashed line) and for the pore filled with each nucleotide (colored full lines); **g** sensitivity histograms for two specific energies (−0.18 and +0.18 eV). Reproduced from Ref. [56] with permission from the Royal Society of Chemistry

the range of −0.06 to 0.0 eV relative to the Fermi energy, which could be attributed to a charge redistribution ($\Delta\rho > 0$) close to the carbon atoms at the left side of the device's pore [57].

The main issue concerning a biomolecule sensor is its capability of identifying each molecule according to a specific property. From the experimental point of view, it can be done by measurements of conductance changes in the device due to its interaction with the target molecules. For evaluate the referred changes were used the sensitivity as defined in Eq. 2. Figure 10g shows the sensitivity at gate voltages $V_g = \pm 0.18\ V$, for the device with each nucleotide at its most stable configuration. Even though, one could present the sensitivity for fully energy spectra, herein, a specific gate voltages were chosen, as at these energies higher contributions of C1 (C2) atoms to the total DOS are noted (Fig. 9c–d). For V_g negative (positive) we noted −3.6%, 16.6%, 29.0%, and 8.3% (−25.2%, −19.9%, 36.2%, and 17.9%) for dAMP, dGMP, dCMP, and dTMP, respectively. These results indicate that device possesses a considerably sensitive resolution to distinguish each nucleotide electrically.

Figure 11 shows the local current for each nucleotide at $V_G = -0.18$ V, where the intensity is represented by the size of the arrows. Combining the sensitivity (Fig. 10g) with the electrical local current of bare device (Fig. 9e), one notes that the dCMP (dAMP) has the higher (lowest) sensitivity leading to bigger (smaller) local current modulation. It is also verified that the current modulation is proportional to sensitivity for dGMP and dTMP. In summary, it was demonstrated that the proposed device can modulate the local current and distinguish each nucleotide electronically.

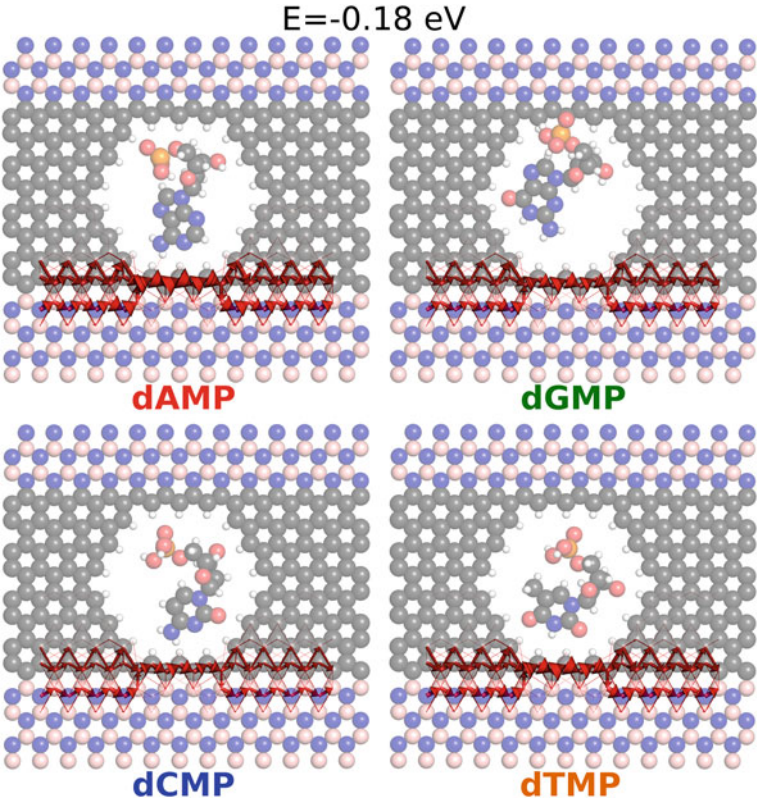

Fig. 11 Local current density modulation is shown for a gate voltage of −0.18 eV. For each nucleotide (dAMP, dGMP, dCMP and dTMP) inside the nanopore, the reference local current (Fig. 2e) is altered due to the different interaction between the molecule and the device. Reproduced from Ref. [56] with permission from the Royal Society of Chemistry

3.4 Surface Application with Graphene Functionalization

The growth or processing of graphene sheets can induce structural defects, which becomes a challenge for graphene-based nanodevice applications. To overcome this issue, the literature [19, 46, 63] has shown that these sheets can be modified with ligands to tune their properties. Surface functionalization can alter how electron transfer processes occur in graphene [16, 35], which can be applied to adjust physical and chemical properties in these systems. Macedo et al. [36] reported an experimental and theoretical study of graphene-modified with 4-carboxyphenyl (4-CP) units, indicating evidence of inhomogeneous charge distribution on the sheets. Here it was employed DFT calculations using GGA exchange-correlation functional, details can be found elsewhere [36].

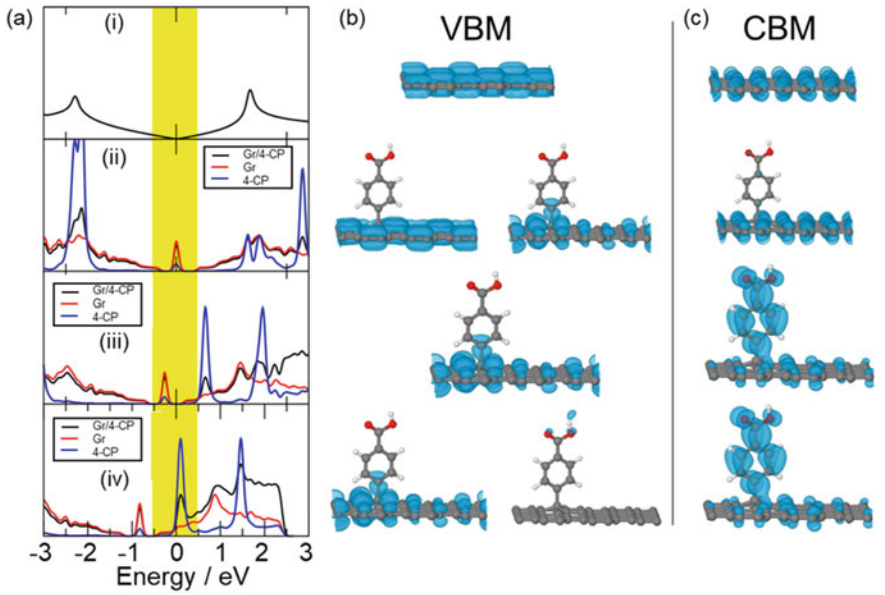

Fig. 12 Computational results of modified graphene. **a** Projected density of states per atom for (i) pristine graphene, graphene functionalized with 4-CP (ii) in a neutral system and in configurations (iii) CS-1 and (iv) CS-2. The yellow dash indicates the region of the Fermi energy between −0.5 and 0.5 eV. Kohn–Sham (KS) wavefunctions at **b** valence band maximum (VBM) and **c** conduction band minimum for cases i, ii, iii, and iv. Because ii and iv are electronically degenerate, both VBM states are shown. Atom colors: C (gray), O (red), H (white), KS wavefunction (blue spheroids). Reproduced from Ref. [36] with permission from the Royal Society of Chemistry

Figure 12 shows the projected density of states (PDOS), also the Kohn-Sham electronic wavefunctions (KS) for the valence band maximum (VBM) and the conduction band minimum (CBM). It was explored the pristine graphene (**i**) and graphene-4CP (**ii**) in a neutral system and in the configurations-1 (CS-1) (**iii**) and -2 (CS-2) (**iv**).

For the pristine graphene was observed the Dirac cone at the Fermi energy, showing π type wavefunction for the VBM and CBM. For the graphene-4CP system (**ii**), there is a hybridization between carbons atoms (graphene) with 4-CP at Fermi energy, since the total number of electrons is odd. The KS states are localized in the molecule/graphene bond in the VBM and its vicinity, while CBM states are similar in comparison to the pristine system. This study also investigates the charge injection, allowing to understand the electron transfer mechanism at the atomic level. The CS-1, denoted as the addition of one extra electron in the system. It generates a small gap and moves the central peak towards the valence band, while its VBM states are similar to the graphene-4CP in the neutral condition. Moreover, the two electrons injection (CS-2) shifts the central peak to −0.9 eV below the Fermi energy. It is worth noting that injection of the extra charge electron induces the non-uniform charge distribution in the graphene-4CP surface, as indicated by the KS VBM and

CBM wavefunctions. These results indicate an anisotropic charge distribution supporting the experimental findings. It also provided the next step, suggesting that these changes are related to the covalent anchoring in the sheet.

4 Conclusion

We presented a discussion regarding interactions between a solid surface and target biomolecules based on quantum mechanic calculations. It was performed DFT in combination with electronic transport method, analysis tools as well as applications examples. It was considered peptide SAMs and biomolecules (DNA) on the three possible detection mechanisms such as: on top, on edge, and nanopore. The on top and on edge systems were also discussed from a functionalization point of view, and their effects to improve devices electronic properties. Nowadays, the computer simulations in nanoscale systems enable a detailed atomic view of the electron transfer process between surfaces and target biomolecules. The future of computer simulations requires multidisciplinary studies between fields such as materials science, solid-state physics, biology, physical chemistry, and bioengineering among others. These advances will have meaningful impacts regarding bioelectronics, contributing to warrant the widest possible dissemination to multidisciplinary scientists, working on the cutting edge of surface science with a strong interest in applications toward nanodevices, which would inspire future experiments.

Acknowledgements The authors acknowledge the financial support of CNPq, FAPESP, FAPES, FAPERJ and INCT-INEO.

References

1. Amorim, R.G., Rocha, A.R., Scheicher, R.H.: Boosting DNA recognition sensitivity of graphene nanogaps through nitrogen edge functionalization. J. Phys. Chem. C (American Chemical Society) **120**(34), 19384–19388 (2016). https://doi.org/10.1021/acs.jpcc.6b04683. Accessed 03 Oct 2021
2. Amorim, R.G., Scheicher, R.H.: Silicene as a new potential DNA sequencing device. Nanotechnology (IOP Publishing) **26**(15), 154002 (2015). https://doi.org/10.1088/0957-4484/26/15/154002. Accessed 03 Oct 2021
3. Amorim, R.G., Zhong, X., Mukhopadhyay, S., Pandey, R., Rocha, A.R., Karna, S.P.: Strain- and electric field-induced band gap modulation in nitride nanomembranes. J. Phys. Cond. Matter **25**(19), 195801 (2013). https://doi.org/10.1088/0953-8984/25/19/195801
4. Bader, R.F.W.: Atoms in Molecules: A Quantum Theory, vol. 22. Inglês. Reprint edição. Oxford University Press, Oxford England: New York (1994)
5. Becke, A.D.: Density-functional thermochemistry. III. The role of exact exchange. J. Chem. Phys. **98**(7), 5648 (1993). ISBN: 0021-9606. https://doi.org/10.1063/1.464913
6. Blöchl, P.E., Först, C.J., Schimpl, J.: Projector augmented wave method: ab initio molecular dynamics with full wave functions. Bull. Mater. Sci. **26**(1), 33–41 (2003). https://doi.org/10.1007/BF02712785

7. Brandbyge, M., Mozos, J.-L., Ordejón, P., Taylor, J., Stokbro, K.: Density-functional method for nonequilibrium electron transport. Phys. Rev. B **65**(16), 165401 (2002). https://link.aps.org/doi/10.1103/PhysRevB.65.165401
8. Brooksby, P.A., Anderson, K.H., Downard, A.J., Abell, A.D.: Electrochemistry of ferrocenoyl beta-peptide monolayers on gold. Langmuir **26**(2), 1334–1339 (2010). http://www.ncbi.nlm.nih.gov/pubmed/19799404. https://doi.org/10.1021/La902402t
9. Cahangirov, S., Topsakal, M., Aktürk, E., Ahin, H., Ciraci, S.: Two- and one-dimensional honeycomb structures of silicon and germanium. Phys. Rev. Lett. **102**(23), 236804 (2009). https://link.aps.org/doi/10.1103/PhysRevLett.102.236804
10. Carvalho, A., Wang, M., Zhu, X., Rodin, A.S., Su, H., Castro Neto, A.H.: Phosphorene: from theory to applications. Nat. Rev. Mater. **1**(11), 1–16 (2016). https://www.nature.com/articles/natrevmats201661. Accessed 03 Oct 2021
11. Di Ventra, M., Taniguchi, M.: Decoding DNA, RNA and peptides with quantum tunnelling. Nat. Nanotechnol. **11**(2) (2016). https://www.nature.com/articles/nnano.2015.320. Accessed 30 Sept 2021
12. Dryfe, R.A.W.: 2D transition metal chalcogenides and van der Waals heterostructures: fundamental aspects of their electrochemistry. Current Opin. Electrochem. Fundamental and Theoretical Electrochemistry • Physical and Nanoelectrochemistry **13**, 119–124 (2019). https://www.sciencedirect.com/science/article/pii/S2451910318302023, Accessed 03 Oct 2021. https://doi.org/10.1016/j.coelec.2018.11.021
13. Eckermann, A.L., Feld, D.J., Shaw, J.A., Meade, T.J.: Electrochemistry of redox-active self-assembled monolayers. Coord. Chem. Rev. **254**(15–16), 1769–1802 (2010). http://www.pubmedcentral.nih.gov/articlerender.fcgi?artid=2885823. https://doi.org/10.1016/J.Ccr.2009.12.023
14. Enkovaara, J., Rostgaard, C., Mortensen, J.J.: Advanced capabilities for materials modelling with Quantum ESPRESSO. J. Phys. Cond. Matter **29**(46), 465901 (2017). http://stacks.iop.org/0953-8984/29/i=46/a=465901. https://doi.org/10.1088/1361-648X/aa8f79
15. Feng, J., Liu, K., Graf, M., Lihter, M., Bulushev, R.D., Dumcenco, D., Alexander, D.T.L., Krasnozhon, D., Vuletic, T., Kis, A., Radenovic, A.: Electrochemical reaction in single layer MoS2: nanopores opened atom by atom. Nano Lett. (American Chemical Society) **15**(5), 3431–3438 (2015). https://doi.org/10.1021/acs.nanolett.5b00768. Accessed 30 Sept 2021
16. Ferrari, A.C., Bonaccorso, F., Fal'ko, V., Novoselov, K.S., Roche, S., Bøggild, P., Borini, S., Koppens, F.H.L., Palermo, V., Pugno, N., Garrido, J.A., Sordan, R., Bianco, A., Ballerini, L., Prato, M., Lidorikis, E., Kivioja, J., Marinelli, C., Ryhönen, T., Morpurgo, A., Coleman, J.N., Nicolosi, V., Colombo, L., Fert, A., Garcia-Hernandez, M., Bachtold, A., Schneider, G.F., Guinea, F., Dekker, C., Barbone, M., Sun, Z., Galiotis, C., Grigorenko, A.N., Konstantatos, G., Kis, A., Katsnelson, M., Vandersypen, L., Loiseau, A., Morandi, V., Neumaier, D., Treossi, E., Pellegrini, V., Polini, M., Tredicucci, A., Williams, G.M., Hong, B.H., Ahn, J.-H., Kim, J.M., Zirath, H., van Wees, B.J., van der Zant, H., Occhipinti, L., Di Matteo, A., Kinloch, I.A., Seyller, T., Quesnel, E., Feng, X., Teo, K., Rupesinghe, N., Hakonen, P., Neil, S.R.T., Tannock, Q., Löfwander, T., Kinaret, J.: Science and technology roadmap for graphene, related two-dimensional crystals, and hybrid systems. Nanoscale **7**(11), 4598–4810 (2015). http://dx.doi.org/10.1039/C4NR01600A
17. Frisch, M.J., Trucks, G.W., Schlegel, H.B., Scuseria, G.E., Robb, M.A., Cheeseman, J.R., Scalmani, G., Barone, V., Mennucci, B., Petersson, G.A., Nakatsuji, H., Caricato, M., Li, X., Hratchian, H.P., Izmaylov, A.F., Bloino, J., Zheng, G., Sonnenberg, J.L., Hada, M., Ehara, M., Toyota, K., Fukuda, R., Hasegawa, J., Ishida, M., Nakajima, T., Honda, Y., Kitao, O., Nakai, H., Vreven, T., Montgomery, J.A. Jr., Peralta, J.E., Ogliaro, F., Bearpark, M., Heyd, J.J., Brothers, E., Kudin, K.N., Staroverov, V.N., Kobayashi, R., Normand, J., Raghavachari, K., Rendell, A., Burant, J.C., Iyengar, S.S., Tomasi, J., Cossi, M., Rega, N., Millam, J.M., Klene, M., Knox, J.E., Cross, J.B., Bakken, V., Adamo, C., Jaramillo, J., Gomperts, R., Stratmann, R.E., Yazyev, O., Austin, A.J., Cammi, R., Pomelli, C., Ochterski, J.W., Martin, R.L., Morokuma, K., Zakrzewski, V.G., Voth, G.A., Salvador, P., Dannenberg, J.J., Dapprich, S., Daniels, A.D., Farkas, Foresman,

J.B., Ortiz, J.V., Cioslowski, J., Fox, D.J.: Gaussian09 Revision D.01. Wallingford, CT, USA (2009)
18. Garcóa, A., Papior, N., Akhtar, A., Artacho, E., Blum, V., Bosoni, E., Brandimarte, P., Brandbyge, M., Cerdá, J.I., Corsetti, F., Cuadrado, R., Dikan, V., Ferrer, J., Gale, J., Garcóa-Fernández, P., Garcóa-Suárez, V.M., Garcóa, S., Huhs, G., Illera, S., Ko- rytár, R., Koval, P., Lebedeva, I., Lin, L., López-Tarifa, P., Mayo, S.G., Mohr, S., Ordejón, P., Postnikov, A., Pouillon, Y., Pruneda, M., Robles, R., Sánchez-Portal, D., Soler, J.M., Ullah, R., Yu, V.W., Junquera, J.: Siesta: recent developments and applications. J. Chem. Phys. (American Institute of Physics) **152**(20), 204108 (2020). https://aip.scitation.org/doi/10.1063/5.0005077. Accessed 01 Oct 2021
19. Georgakilas, V., Otyepka, M., Bourlinos, A.B., Chandra, V., Kim, N., Christian Kemp, K., Hobza, P., Zboril, R., Kim, K.S.: Functionalization of graphene: covalent and non-covalent approaches, derivatives and applications. Chem. Rev. **112**(11), 6156–6214 (2012). PMID: 23009634. https://doi.org/10.1021/cr3000412
20. Giannozzi, P., Baroni, S., Bonini, N., Calandra, M., Car, R., Cavazzoni, C., Ceresoli, D., Chiarotti, G.L., Cococcioni, M., Dabo, I., Corso, A.D., De Gironcoli, S., Fabris, S., Fratesi, G., Gebauer, R., Gerstmann, U., Gougoussis, C., Kokalj, A., Lazzeri, M., Martin-Samos, L., Marzari, N., Mauri, F., Mazzarello, R., Paolini, S., Pasquarello, A., Paulatto, L., Sbraccia, C., Scandolo, S., Sclauzero, G., Seitsonen, A.P., Smogunov, A., Umari, P., Wentzcovitch, R.M., Dal Corso, A., Fabris, S., Fratesi, G., De Gironcoli, S., Gebauer, R., Gerstmann, U., Gougoussis, C., Kokalj, A., Lazzeri, M., Martin-Samos, L., Marzari, N., Mauri, F., Mazzarello, R., Paolini, S., Pasquarello, A., Paulatto, L., Sbraccia, C., Scandolo, S., Sclauzero, G., Seitsonen, A.P., Smogunov, A., Umari, P., Wentzcovitch, R.M., Dal Corso, A., De Gironcoli, S., Fabris, S., Fratesi, G., Gebauer, R., Gerstmann, U., Gougoussis, C., Kokalj, A., Lazzeri, M., Martin-Samos, L., Marzari, N., Mauri, F., Mazzarello, R., Paolini, S., Pasquarello, A., Paulatto, L., Sbraccia, C., Scandolo, S., Sclauzero, G., Seitsonen, A.P., Smogunov, A., Umari, P., Wentzcovitch, R.M.: QUANTUM ESPRESSO: a modular and open-source software project for quantum simulations of materials. J. Phys. Cond. Matter **21**(39), 395502 (19 pp) (2009). http://www.ncbi.nlm.nih.gov/pubmed/21832390%20. http://arxiv.org/abs/0906.2569. https://doi.org/10.1088/0953-8984/21/39/395502
21. Grimme, S., Hansen, A., Brandenburg, J.G., Bannwarth, C.: Dispersion-corrected mean-field electronic structure methods. Chem. Rev. (American Chemical Society) **116**(9), 5105–5154 (2016). https://doi.org/10.1021/acs.chemrev.5b00533. Accessed 16 Feb 2021
22. Hassan, A., Macedo, L.J.A., Mattioli, I.A., Rubira, R.J.G., Constantino, C.J.L., Amorim, R.G., Lima, F.C.D.A., Crespilho, F.N.: A three component-based van der Waals surface vertically designed for biomolecular recognition enhancement. Electrochim. Acta **376**, 138025 (2021). https://www.sciencedirect.com/science/article/pii/S0013468621003157. Accessed 03 Oct 2021. https://doi.org/10.1016/j.electacta.2021.138025
23. Heerema, S.J., Dekker, C.: Graphene nanodevices for DNA sequencing. Nat. Nanotechnol. **11**(2) (2016). https://www.nature.com/articles/nnano.2015.307. Accessed 30 Sept 2021
24. Henkelman, G., Arnaldsson, A., Jónsson, H.: A fast and robust algorithm for bader decomposition of charge density. Comput. Mater. Sci. **36**(3), 354–360 (2006)
25. Heyd, J., Scuseria, G.E., Ernzerhof, M.: Hybrid functionals based on a screened Coulomb potential. J. Chem. Phys. (American Institute of Physics) **118**(18), 8207–8215 (2003). https://aip.scitation.org/doi/10.1063/1.1564060. Accessed 01 Oct 2021
26. Hohenberg, P., Kohn, W.: Inhomogeneous electron gas. Phys. Rev. **136**(3B), B864–B871 (1964). http://link.aps.org/doi/10.1103/PhysRev.136.B864
27. Kai, M., Takeda, K., Morita, T., Kimura, S.: Distance dependence of long-range electron transfer through helical peptides. J. Pept. Sci. **14**(2), 192–202 (2008). http://www.ncbi.nlm.nih.gov/pubmed/18035857. https://doi.org/10.1002/Psc.974
28. Kohn, W., Sham, L.J.: Self-consistent equations including exchange and correlation effects. Phys. Rev. **140**(4A), A1133–A1138 (1965). http://link.aps.org/doi/10.1103/PhysRev.140.A1133

29. Kresse, G., Furthmüller, J.: Efficient iterative schemes for ab initio total-energy calculations using a plane-wave basis set. Phys. Rev. B (American Physical Society) **54**(16), 11169–11186 (1996). https://link.aps.org/doi/10.1103/PhysRevB.54.11169. Accessed 01 Oct 2021
30. Kwok, H., Briggs, K., Tabard-Cossa, V.: Nanopore fabrication by controlled dielectric breakdown. PLOS ONE (Public Library of Science) **9**(3), e92880 (2014). https://journals.plos.org/plosone/article?id=10.1371/journal.pone.0092880. Accessed 30 Sept 2021
31. Lee, J.-H., Choi, Y.-K., Kim, H.-J., Scheicher, R.H., Cho, J.-H.: Physisorption of DNA nucleobases on h-BN and graphene: vdW-corrected DFT calculations. J. Phys. Chem. C **117**(26), 13435–13441 (2013)
32. Liang, L., Wei, H., Xue, Z., Shen, J.-W.: Theoretical study on the interaction of nucleotides on two-dimensional atomically thin graphene and molybdenum disulfide. FlatChem **2**, 8–14 (2017)
33. Lima, F.C.D.A., Calzolari, A., Iost, R.M., Crespilho, F.N., Petrilli, H.M., Caldas, M.J., Iost, R.M., Crespilho, F.N., Petrilli, H.M., Lima, F.C.D.A., Caldas, M.J., Iost, R.M., Crespilho, F.N., Petrilli, H.M.: Electronic structure of self-assembled monolayers modified with ferrocene on a gold surface: evidence of electron tunneling. J. Phys. Chem. C **118**(40), 23111–23116 (2014). http://pubs.acs.org/doi/abs/10.1021/jp506425c
34. Liu, N., Bo, G., Liu, Y., Xu, X., Du, Y., Dou, S.X.: Recent progress on germanene and functionalized germanene: preparation, characterizations, applications, and challenges. Small **15**(32), 1805147 (2019). https://onlinelibrary.wiley.com/doi/abs/10.1002/smll.201805147. Accessed 03 Oct 2021
35. Macedo, L.J.A., Iost, Ayaz Hassan, R.M., Balasubramanian, K., Crespilho, F.N.: Bioelectronics and interfaces using monolayer graphene. ChemElectroChem **6**(1), 31–59 (2019). https://onlinelibrary.wiley.com/doi/abs/10.1002/celc.201800934. Accessed 03 Oct 2021
36. Macedo, L.J.A., Lima, F.C.D.A., Amorim, R.G., Freitas, R.O., Yadav, A., Iost, R.M., Balasubramanian, K., Crespilho, F.N.: Interplay of non-uniform charge distribution on the electrochemical modification of graphene. Nanoscale (The Royal Society of Chemistry) **10**(31), 15048–15057 (2018). https://pubs.rsc.org/en/content/articlelanding/2018/nr/c8nr03893g. Accessed 30 Sept 2021. https://doi.org/10.1039/C8NR03893G
37. Malak, R.A., Gao, Z., Wishart, J.F., Isied, S.S.: Long-range electron transfer across peptide bridges: the transition from electron superexchange to hopping. J. Am. Chem. Soc. **126**(43), 13888–13889 (2004). http://www.ncbi.nlm.nih.gov/pubmed/15506726. https://doi.org/10.1021/Ja0401040
38. Mandal, H.S., Kraatz, H.-B.: Electron transfer across α-helical peptides: potential influence of molecular dynamics. J. Chem. Phys. **326**(1), 246–251 (2006). http://linkinghub.elsevier.com/retrieve/pii/S0301010406000498. https://doi.org/10.1016/J.Chemphys.2006.01.010
39. Mandal, H.S., Kraatz, H.-B.: Electron transfer mechanism in helical peptides. J. Phys. Chem. Lett. **3**(6), 709–713 (2012). http://pubs.acs.org/doi/abs/10.1021/jz300008s
40. MartiĆ, S., Labib, M., Shipman, P.O., Kraatz, H.-B.: Ferrocene-peptido conjugates: from synthesis to sensory applications. Dalton Trans. **40**(28), 7264–7290 (2011). http://www.ncbi.nlm.nih.gov/pubmed/21483964. https://doi.org/10.1039/C0dt01707h
41. Min, S.K., Kim, W.Y., Cho, Y., Kim, K.S.: Fast DNA sequencing with a graphene-based nanochannel device. Nat. Nanotechnol. **6**(3), 162–165 (2011). https://www.nature.com/articles/nnano.2010.283. Accessed 05 Oct 2021. https://doi.org/10.1038/nnano.2010.283
42. Morita, T., Kimura, S.: Long-range electron transfer over 4 nm governed by an inelastic hopping mechanism in self-assembled mono-layers of helical peptides. J. Am. Chem. Soc. **125**(29), 8732–8733 (2003). http://www.ncbi.nlm.nih.gov/pubmed/12862461. https://doi.org/10.1021/Ja034872n
43. Neese, F.: The ORCA program system. WIREs Comput. Mol. Sci. **2**(1) (2012). https://onlinelibrary.wiley.com/doi/abs/10.1002/wcms.81. Accessed 30 Sept 2021
44. Novoselov, K.S., Geim, A.K., Morozov, S.V., Jiang, D., Zhang, Y., Dubonos, S.V., Grigorieva, I.V., Firsov, A.A.: Electric field effect in atomically thin carbon films. Science (American Association for the Advancement of Science) **306**(5696), 666–669 (2004). https://www.science.org/lookup/doi/10.1126/science.1102896. Accessed 23 Sept 2021

45. Orlowski, G.A., Chowdhury, S., Long, Y.-T., Sutherland, T.C., Kraatz, H.-B.: Electrodeposition of ferrocenoyl peptide disul-fides. Chem. Commun. **2**(10), 1330–1332 (2005). http://www.ncbi.nlm.nih.gov/pubmed/15742068. https://doi.org/10.1039/B415278f
46. Paulus, G.L.C., Wang, Q.H., Strano, M.S.: Covalent electron transfer chemistry of graphene with diazonium salts. Acc. Chem. Res. **46**(1), 160–170 (2013). PMID: 22946516. https://doi.org/10.1021/ar300119z
47. Pawlowski, J., Juhaniewicz, J., Tymecka, D., Sek, S.: Electron transfer across α-helical peptide monolayers: importance of inter-chain coupling. Langmuir **28**(50), 17287–17294 (2012). http://www.ncbi.nlm.nih.gov/pubmed/23181704. https://doi.org/10.1021/La302716n
48. Perdew, J.P., Zunger, A.: Self-interaction correction to density-functional approximations for many-electron systems. Phys. Rev. B **23**(10), 5048–5079 (1981). https://link.aps.org/doi/10.1103/PhysRevB.23.5048. https://doi.org/10.1103/PhysRevB.23.5048
49. Perdew, J.P., Burke, K., Ernzerhof, M.: Generalized gradient approximation made simple. [Phys. Rev. Lett. **77**, 3865 (1996)]. Phys. Rev. Lett. **78**(7), 1396–1396 (1997). http://link.aps.org/doi/10.1103/PhysRevLett.78.1396
50. Perdew, J.P., Ruzsinszky, A., Csonka, G.I., Vydrov, O.A., Scuseria, G.E., Constantin, L.A., Zhou, X., Burke, K.: Restoring the density-gradient expansion for exchange in solids and surfaces. Phys. Rev. Lett. **100**(13), 136406 (2008). https://doi.org/10.1103/PhysRevLett.100.136406
51. Polo, F., Antonello, S., Formaggio, F., Toniolo, C., Maran, F.: Evidence against the hopping mechanism as an important electron transfer pathway for conformationally constrained oligopeptides. J. Am. Chem. Soc. **127**(2), 492–493 (2005). http://www.ncbi.nlm.nih.gov/pubmed/15643851. https://doi.org/10.1021/Ja043607e
52. Postma, H.W.: Rapid sequencing of individual DNA molecules in graphene nanogaps. Nano Lett. (American Chemical Society) **10**(2), 420–425 (2010). https://doi.org/10.1021/nl9029237. Accessed 11 Oct 2021
53. Prasongkit, J., Grigoriev, A., Pathak, B., Ahuja, R., Scheicher, R.H.: Transverse conductance of DNA nucleotides in a graphene nanogap from first principles. Nano Lett. (American Chemical Society) **11**(5), 1941–1945 (2011). https://doi.org/10.1021/nl200147x. Accessed 23 Sept 2021
54. Rocha, A.R., García-Suárez, V.M., Bailey, S., Lambert, C., Ferrer, J., Sanvito, S.: Spin and molecular electronics in atomically generated orbital landscapes. Phys. Rev. B **73**(8), 085414 (2006). https://link.aps.org/doi/10.1103/PhysRevB.73.085414
55. Shah, A., Adhikari, B., Martic, S., Munir, A., Shahzad, S., Ahmad, K., Kraatz, H.: Electron transfer in peptides. Chem. Soc. Rev. **44**, 1015–1027 (2015). https://doi.org/10.1039/C4CS00297K
56. Souza, F.A.L. de, Amorim, R.G., Scopel, W.L., Scheicher, R.H.: Electrical detection of nucleotides via nanopores in a hybrid graphene/h-BN sheet. Nanoscale (The Royal Society of Chemistry) **9**(6), 2207– 2212 (2017). https://pubs.rsc.org/en/content/articlelanding/2017/nr/c6nr07154f. Accessed 30 Sept 2021. https://doi.org/10.1039/C6NR07154F
57. Souza, F.A.L. de, Amorim, R.G., Scopel, W.L., Scheicher, R.H.: Controlled current confinement in interfaced 2D nanosensor for electrical identification of DNA. Phys. Chem. Chem. Phys. (The Royal Society of Chemistry) **21**(45), 24884–24890 (2019). https://pubs.rsc.org/en/content/articlelanding/2019/cp/c9cp03950c. Accessed 11 Oct 2021. https://doi.org/10.1039/C9CP03950C
58. de Souza, F.A.L., Amorim, R.G., Scopel, W.L., Scheicher, R.H.: Nano-structured interface of graphene and h-BN for sensing applications. Nanotechnology **27**(36), 365503 (2016). https://doi.org/10.1088/0957-4484/27/36/365503
59. Su, N.Q., Xu, X.: Development of new density functional approximations. Ann. Rev. Phys. Chem. **68**(1), 155–182 (2017). PMID: 28226221. https://doi.org/10.1146/annurev-physchem-052516-044835
60. Szabo, A., Szabo, J.: Modern Quantum Chemistry: Introduction to Advanced Electronic Structure Theory. Inglês. Revised ed. edição. Dover Publications, Mineola, N.Y. (1996)
61. Takeda, K., Morita, T., Kimura, S.: Effects of mono-layer structures on long-range electron transfer in helical peptide monolayer. J. Phys. Chem. B **112**(40), 12840–12850 (2008). http://www.ncbi.nlm.nih.gov/pubmed/18793017. https://doi.org/10.1021/Jp805711v

62. Vanderbilt, D.: Optimally smooth norm-conserving pseudopotentials. Phys. Rev. B **32**(12), 8412–8415 (1985). https://link.aps.org/doi/10.1103/PhysRevB.32.8412
63. Wang, Q.H., Shih, C.-J., Paulus, G.L.C., Strano, M.S.: Evolution of physical and electronic structures of bilayer graphene upon chemical functionalization. J. Am. Chem. Soc. **135**(50), 18866–18875 (2013). PMID: 24266808. https://doi.org/10.1021/ja4083914
64. Wang, Z.-Q., Lü, T.-Y., Wang, H.-Q., Feng, Y.P., Zheng, J.-C.: Review of borophene and its potential applications. Front. Phys. **14**(3), 33403 (2019). https://doi.org/10.1007/s11467-019-0884-5. Accessed 03 Oct 2021
65. Watanabe, J., Morita, T., Kimura, S.: Effects of dipole moment, linkers, and chromophores at side chains on long-range electron transfer through helical peptides. J. Phys. Chem. B **109**(30), 14416–14425 (2005). http://www.ncbi.nlm.nih.gov/pubmed/16852814. https://doi.org/10.1021/Jp051592g
66. Yu, M., Trinkle, D.R.: Accurate and efficient algorithm for bader charge integration. J. Chem. Phys. **134**(6), 064111 (2011)
67. Zhang, L., Yang, Z., Gong, T., Pan, R., Wang, H., Guo, Z., Zhang, H., Fu, X.: Recent advances in emerging Janus two-dimensional materials: from fundamental physics to device applications. J. Mater. Chem. A (The Royal Society of Chemistry) **8**(18), 8813–8830 (2020). https://pubs.rsc.org/en/content/articlelanding/2020/ta/d0ta01999b. Accessed 03 Oct 2021. https://doi.org/10.1039/D0TA01999B